WELDING RESEARCH

SUPPLEMENT TO THE *WELDING JOURNAL*, NOVEMBER 1998
Sponsored by the American Welding Society and the Welding Research Council

RESEARCH/DEVELOPMENT/RESEARCH/DEVELOPMENT/RESEARCH/DEVELOPMENT/RESEARCH/DEVELOPMENT

Analysis of Residual Stresses in Al-Li Repair Welds and Mitigation Techniques

Thermal stretching, a novel repair technique, is proposed as a way to reduce residual stresses in repair welds

BY P. DONG, J. K. HONG AND P. ROGERS

ABSTRACT. In this paper, the recent results based on a comprehensive study on repair weld residual stresses are presented. Advanced finite element techniques were used to characterize the residual stress evolution in Al-Li alloy weldments, particularly under repair welding conditions. The present analysis procedures considered three-dimensional residual stress characteristics in the repair welds using a shell element model. Local residual stress details were analyzed by a generalized plane-strain model with prescribed translation and rotation conditions established from the global shell element model. Experimental residual stress measurements were conducted using X-ray diffraction methods. A good agreement between the finite element results and experimental measurements was obtained. Finally, a novel welding repair procedure (termed as a "thermal stretching" technique) was proposed to mitigate the weld residual stresses in repair.

Introduction

It is well established that residual stresses result from localized heating and cooling and mechanical restraint conditions during and after welding. During repair welding, material near and within the weld fusion zone undergoes severely restrained thermomechanical deformation. Consequently, residual stresses near a repair weld can be significantly higher than those in an original weld before repair. In addition, there has been a great deal of evidence that residual stresses due to weld repair can significantly impact the structural integrity of the welded structures (Ref. 1).

There have been numerous studies on weld residual stresses. Some comprehensive discussions on this subject can be found in Masubuchi (Ref. 1) where a large amount of experimental data was documented and analyzed. As finite element methods gain popularity in solving complex thermoplasticity problems, such as those involved in welding-induced residual stresses, a better understanding of the residual stress development can be achieved through a proper application of these powerful methods. Representative work along this line is that by Ueda, *et al.* (Ref. 2), and Kim, *et al.* (Ref. 3), for multipass welds and by Rybicki, *et al.* (Ref. 4) and Brust, *et al.* (Refs. 5, 6), for pipe girth welds. In addition, various modeling techniques have been proposed to address some specific concerns over thermal and mechanical aspects of the finite element procedures associated with residual stress analysis (Refs. 7–11). In addition, some of the more recent publications considered solidification effects, for example, by Choi and Mazumder (Ref. 12) on residual stresses in 304 stainless steel weldments and by Oddy, *et al.* (Ref. 13), on transformation plasticity effects in pressure-vessel steel. Some of the additional modeling issues were discussed in light of numerical predictions for gas tungsten arc (GTA) welds, and neutron diffraction measurements (based on residual elastic strains) were discussed by Mahin, *et al.* (Ref. 14).

As commercial finite element codes become increasingly available, the use of such general-purpose codes for residual stress analysis has become highly desirable. This is because not only can residual stress analysis procedures based on commercial codes be readily adapted to practical applications, but also the development effort can be focused only on welding-specific issues by taking advantage of the existing computational architecture already available in commercial

KEY WORDS

Al-Li Alloys
Finite Element Analysis
Mitigation Techniques
Multipass Welds
Repair Weld
Residual Stresses
Shell Element Model
Thermal Stretching Technique

P. DONG and J. K. HONG are with the Center for Welded Structures Research, Battelle, Columbus, Ohio. P. ROGERS is with Marshall Space Flight Center, Huntsville, Ala.

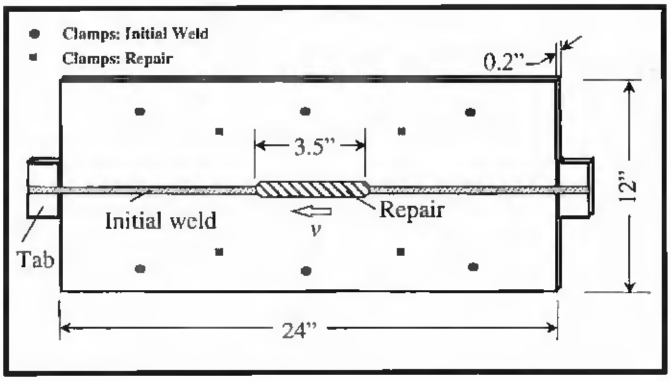

Fig. 1 — Aluminum-lithium panel specimen with a repair weld.

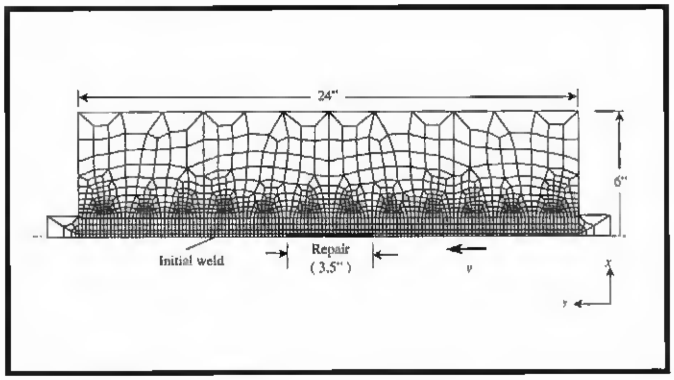

Fig. 2 — Half-panel shell/plate element model.

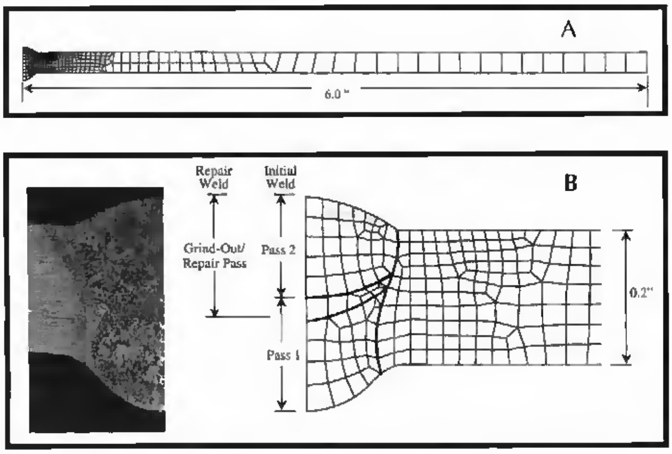

Fig. 3 — Two-dimensional cross section model. A — Entire model; B — fusion profile micrograph and mesh design in weld area.

codes. Along this line, some insightful results on weld residual stresses have been obtained (Refs. 11–18) where the effects of multipass welds were simulated directly using a commercial code, *ABAQUS* (Ref. 19), with a user-developed welding heat source model. However, it should be noted that very few commercial finite element codes are designed for modeling important phenomena peculiar to welding, such as melting/remelting and metal deposition effects (Ref. 17). An effective remedy for this has been implemented by the development of a proper material model in the form of user subroutines (Ref. 20), with which additional capabilities can also be obtained in modeling multipass welds and 3-D effects using special shell or plate element models (Ref. 21). The availability of such facilities makes it possible to analyze the detailed development of the residual stresses in repair welds in complex engineering components, which typically requires the incorporation of 3-D effects that have been traditionally assumed negligible in 2-D and axisymmetric models in the past (Refs. 4–6, 15, 16).

A detailed study on weld residual stresses in aluminum-lithium (Al-Li) weldments follows. Special attention is given to the residual stress development in repair welds. An advanced finite element procedure using both 3-D shell/plate and 2-D generalized plane-strain element models is discussed. Experimental residual stress data are also compared with finite element predictions. The implications on structural integrity are discussed in Refs. 22 and 23. A potential residual stress mitigation technique is also presented based on the detailed evolution of residual stresses in repair welds from this investigation.

Residual Stress Analysis

Problem Definition

As shown in Fig. 1, the Al-Li panel specimen with a repair weld was prepared for X-ray diffraction residual stress measurements after both the initial weld and the repair weld. For the initial weld, six C clamps were used with three on each side of the weld at positions as indicated, while four clamps were used for the repair. The initial weld was performed using an automatic two-pass variable polarity plasma arc (VPPA) process (with welding wire).

The repair weld was performed with the manual GTAW process (with welding wire). The details about the welding process parameters are given in Rogers, *et al.* (Ref. 23). The welding repair procedure involved grinding out approximately half the weld thickness to remove defects and filling the resulting groove with two passes using a manual GTAW process (with welding wire). The welding arc was assumed to travel from the right to the left, as indicated.

Computational Procedures

Finite element simulation of the residual stress development in repair welds typically requires the consideration of 3-D effects in a component. This can be accomplished with a combined approach using shell/plate and 2-D models (Refs. 17, 20, 21). Such a simplified approach was necessary for the application of concern since analysis using 3-D solid-element models would have been extremely time consuming and cumbersome for simulating multipass repair welding. This analysis procedure can be briefly described as follows: 1) A special composite shell element model (Ref. 21) is used to establish global residual stress distributions in an actual weldment considering moving arc metal deposition effects; 2) a 2-D cross-section model of generalized plane-strain elements is then used to compute local residual stress details at a specified cross section along the weld simulated in the shell model. In the 2-D cross-section model, a set of averaged nodal displacements from the shell model is specified in terms of both cross-section rotations and translations. In this study, the averaged final nodal displacements from the shell model were used as out-of-plane boundary conditions for the 2-D cross-section model.

Computational Models

As such, two types of finite element models were used in the present study. A shell/plate element model is shown in

Fig. 2, representing the upper half of the panel specimen shown in Fig. 1. Symmetry conditions with respect to the y-z plane were imposed along the weld centerline. In addition, clamping actions were simulated using fixed displacement (u_z) boundary conditions. The first row of elements from the bottom represents the weld material. Four-node shell elements with six degrees of freedom were used. Five through-thickness integration points were used in both thermal and mechanical analyses (Ref. 19). The moving arc effects were simulated using a distributed heat flux model coded as a user subroutine in *ABAQUS* (Ref. 19). With this shell/plate element model, only the second pass of the two-pass initial weld was modeled to simplify the analysis procedure (for discussion on using shell/plate element to model multipass weld effects, see Ref. 21). Previous results (Refs. 2, 3, 18) have demonstrated that the last pass typically dominates the residual stress distribution in multipass welds, at least for a region close to the last pass. The 3.5-in. (0.14-mm) repair weld was simulated after the initial weld residual stresses were obtained. The displacement characteristics obtained at the mid-length of the initial weld was used to describe the generalized plane-strain conditions for a 2-D model with which local residual stress details were investigated further.

A cross-section model is shown in Fig. 3. Transient heat flow solutions were carried out for both initial and repair weld passes by using combined body and surface fluxes so that the predicted fusion zone for each pass was approximately the same as the experimentally observed one — Fig. 3B. "Element rebirth" techniques (Ref. 16) were used to simulate the effects of the two-pass initial weld. (A more robust technique for modeling multipass welds in complex structures is discussed in detail in Ref. 20, and the results for the present applications were essentially the same.) The repair weld was simulated in a similar manner: 1) The elements representing grind-out material (two enclosed areas at the top in Fig. 3B) were removed; 2) these elements were then reintroduced as one repair pass with a specified heat input consistent with the GTA welding parameters.

Material Model

The thermal-physical properties at room temperature are given in Table 1. Since high-temperature properties were not available for the Al-Li alloy of concern, they were assumed to be of typical 2000-series aluminum alloys.

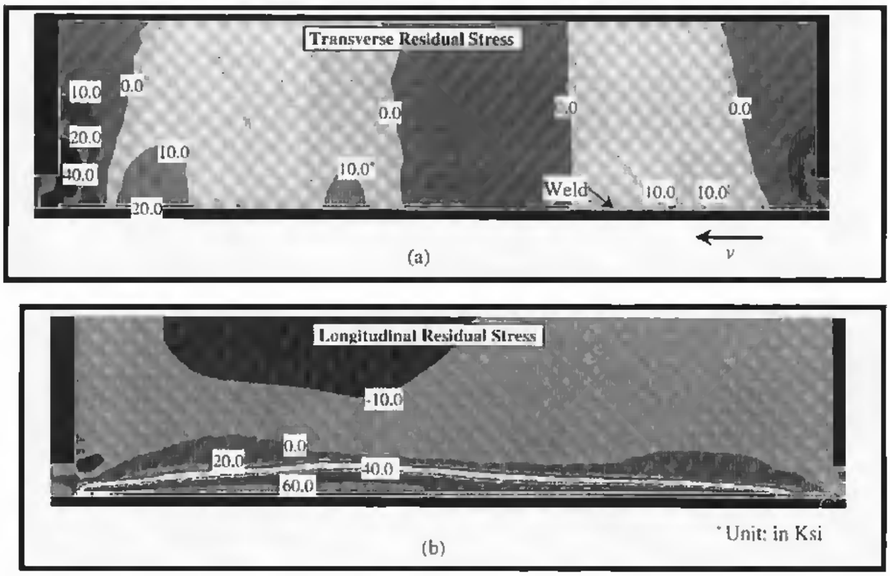

Fig. 4 — Residual stress distributions for the initial weld. A — Transverse residual stress ; B — longitudinal residual stress.

Table 1 — Room Temperature Material Properties

	k (Btu/in./°F)	C_p (Btu/lb/°F)	ρ (lb/in.^{3})	α (in./in.)	E (ksi)	ν	σ_y (ksi)
Base metal	0.003156	0.214	0.976	14.1×10^{-6}	11,600	0.3153	63
Filler metal	0.003156	0.214	0.976	14.1×10^{-6}	10,500	0.3153	40

The room-temperature tensile properties for both base metal and filler material combinations are also given in Table 1. Von Mises yield criterion with associated flow rule was used. Elastic perfectly plastic behavior was assumed in the analysis. Since there were no data available for yield stress vs. plastic strain at elevated temperatures for both the base material and weld metal of concern, a linear relationship was assumed for both yield stress and Young's Modulus, linearly decreasing from the room-temperature values to the melting temperature. It was assumed that at the melting temperature, the yield strengths and Young's Modulus were reduced by two orders of magnitude from their room temperature values. Past experience has shown that this is adequate as far as residual stresses are concerned, since the residual stress state tends to be controlled primarily by the room temperature material properties.

With both shell/plate and 2-D cross-section models, a sequentially coupled thermal-mechanical procedure was used. With such a procedure, thermal analysis was first performed to obtain the temperature history during and after welding, and then thermo-mechanical analysis was conducted with respect to the entire temperature history to obtain the corresponding residual stress state.

Results and Discussion

Initial Welds

The shell/plate element model in Fig. 2 was first used to analyze the residual stress development for the initial weld. The predicted residual stress distributions are shown in Fig. 4. Note that the start and stop positions are located on outer ends of the transition tabs. It is interesting to note that the transverse residual stresses show a strong variation along the entire weld length while the longitudinal residual stresses remain essentially constant along the weld length except near the start/stop positions. The transverse residual stresses along a line at 0.3 in. (7.6 mm) from the weld centerline are shown in Fig. 5. Residual stress measurements (in symbols) were also obtained with the X-ray diffraction technique at four equally spaced positions along this line for the last half of the 24-in. (610-mm) initial weld. It should be noted that the shell/plate element model was only intended to capture some of the global residual stress characteristics. Nevertheless, the agreement between the measured and predicted results is reasonable.

Such residual stress distribution characteristics are not completely unexpected. It is well established that the lon-

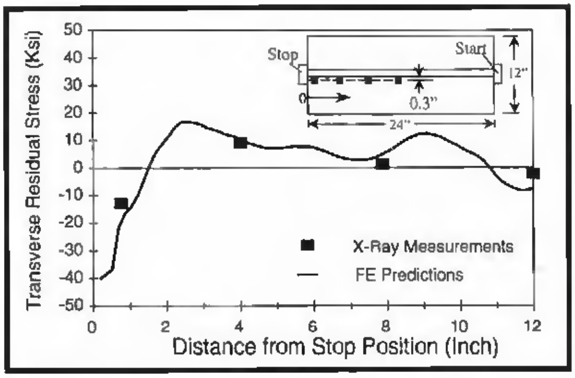

Fig. 5 — Transverse residual stress distribution along weld length.

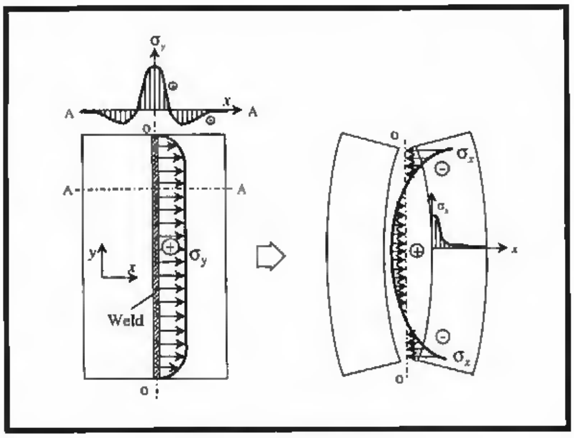

Fig. 6 — Transverse residual stresses due to longitudinal restraint.

gitudinal residual stresses are primarily dominated by the workpiece's restraint in the longitudinal direction, and their typical distributions along an initial weld are illustrated in Fig. 6. The transverse residual stress distribution, however, can be attributed to both longitudinal and transverse restraints. A simple free-body diagram with an imaginary cut along the weld centerline is used in Fig. 6 to demonstrate the contribution of weld longitudinal shrinkage to the variation of the transverse residual stress along the weld as shown in Figs. 4 and 5. Without quantifying this important residual stress feature for the transverse residual stress component (Fig. 4A), analysis results from a 2-D model may not be correctly interpreted.

To investigate the detailed local residual stress distributions, the 2-D generalized plane-strain element model (Fig. 3) was used along with prescribed displacement conditions obtained from the shell/plate element model, as discussed above. The residual stress results on the top surface are plotted as a function of distance from the weld centerline in Fig. 7, in which experimental X-ray diffraction measurements are plotted in symbols. The predicted longitudinal stresses in the weld area (Fig. 7A) clearly indicates the weld metal undermatch effects (*i.e.*, its yield strength was lower than the base material's by about 45%). The maximum tensile stress occurs within the HAZ region due to the high yield strength of the base material. The agreement between the predictions and measurements was considered reasonable, particularly away from the weld.

The transverse residual stress results on the top surface are shown in Fig. 7B. Within the fusion zone, the transverse component is small. The transverse residual stress reaches its maximum at the weld interface and is followed with a rapid decrease. Some oscillations can be seen for some distance farther away from the weld before the transverse component gradually approaches zero. It should be noted that clamp positions were located at about 2.5 in. (63.5 mm) away from the weld centerline and that its effects can be clearly seen in the predicted results, although both the finite element and X-ray measurement results were obtained under conditions with clamps being released. The X-ray diffraction measurement results followed the same trend.

Repair Welds

Once the initial weld residual stress field was established, as discussed in the previous section, the repair welding was simulated using the procedures described previously. The results are also summarized in Fig. 7. The change in longitudinal residual stresses due to repair is not noticeable. However, the transverse residual stress component shows an overall increase, particularly away from the fusion zone. This trend was further confirmed by the X-ray measurements, shown in symbols (triangles) in Fig. 7B. To illustrate the detailed transverse residual stress development over the repair welding process, the residual stress dis-

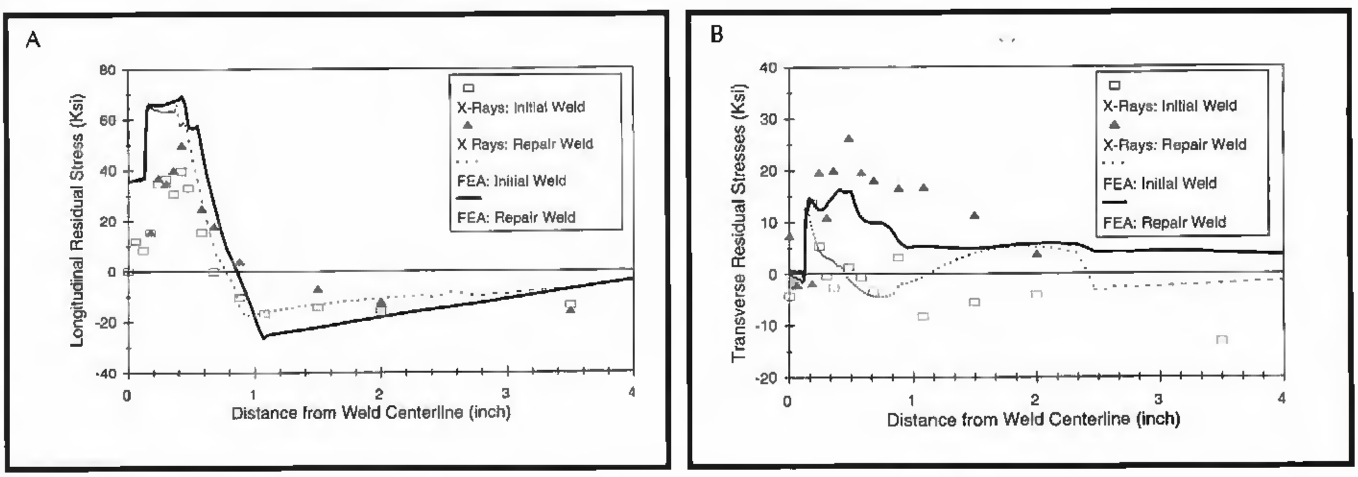

Fig. 7 — Comparison of finite element predictions and X-ray measurements at panel mid-length. A — Longitudinal residual stress; B — transverse residual stress.

tributions after the initial weld, groove preparation (grind out) and repair are summarized in Fig. 8. The solid line represents the residual stress distribution after the initial weld. After grinding out the material within the initial weld as indicated in Fig. 3, free surface effects were introduced within the original weld. As a result, the initial transverse residual stress (solid lines) was gradually reduced to zero as the newly created surface is approached, as indicated by the long-dashed lines. Furthermore, the residual stress peak was shifted to about 0.5 in. (12.7 mm) away from the weld interface. After repair, a significant increase in residual stress in the nearby area immediately outside of the repair weld can be seen, as shown by the short-dashed lines.

The shell/plate element model was also used to investigate the global features of the repair weld residual stresses for the entire panel specimen. Figure 9 shows the residual stress distributions after weld repair. Within the repair length (in the middle of the panel specimen), the transverse stresses become highly tensile (more than 40 ksi), in contrast to Fig. 4A. Immediately outside the repair weld length, the transverse stresses become compressive. Again, the longitudinal residual stress remains relatively uniform along the repair weld length.

Mitigation Technique

The presence of high tensile transverse residual stresses within the repair weld can have a significant impact on the structural integrity of the component (Ref. 22). It is important that potential mitigation techniques be investigated so that repair weld residual stress effects on structural integrity can be minimized. For the present applications, this can be achieved by a certain arrangement of localized in-plane heating and/or cooling with a detailed consideration of the residual stress evolution process in the repair welds. It should be noted that some early efforts by means of localized heating/cooling were primarily used for mitigating buckling-type distortions — for example, low-stress nondistortion (LSND) welding techniques proposed by Guan, *et al.* (Ref. 24), for butt joints and "thermal tensioning" techniques by Michaleris and Sun (Ref. 25). In both cases, the longitudinal compressive residual stresses along the weld, which act as internal buckling load, must be reduced in order to mitigate buckling distortions. As far as residual stress mitigation techniques are concerned, one of the well-known methods is the heat sink welding technique for multipass girth welds developed by Brust, *et al.* (Refs. 5, 6). The heat-sink welding techniques utilized intensified temperature gradients generated by cooling the pipe inner surface after the first pass to mitigate the final tensile residual stresses near the pipe inner surface. The method has been successfully implemented in preventing residual-stress-induced stress corrosion cracking on the inner surface of a pipe weld in the

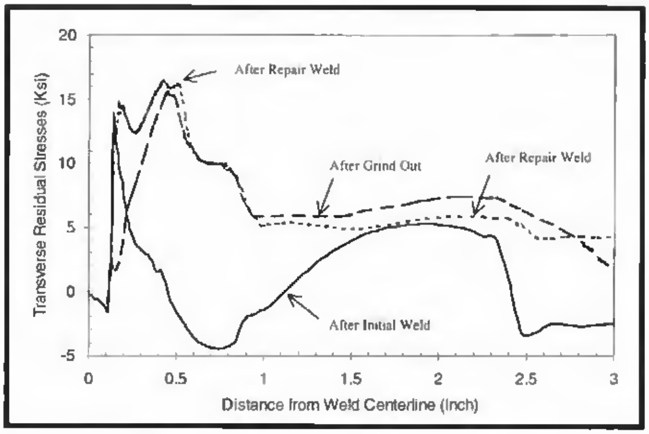

Fig. 8 — Predicted residual stress evolution during and after repair.

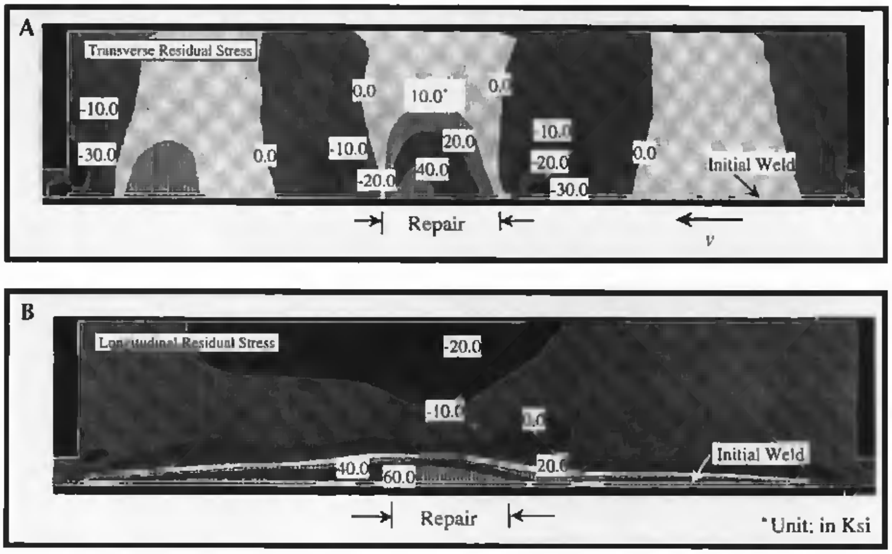

Fig. 9 — Residual stress distributions. A — Transverse residual stress; B — longitudinal residual stress.

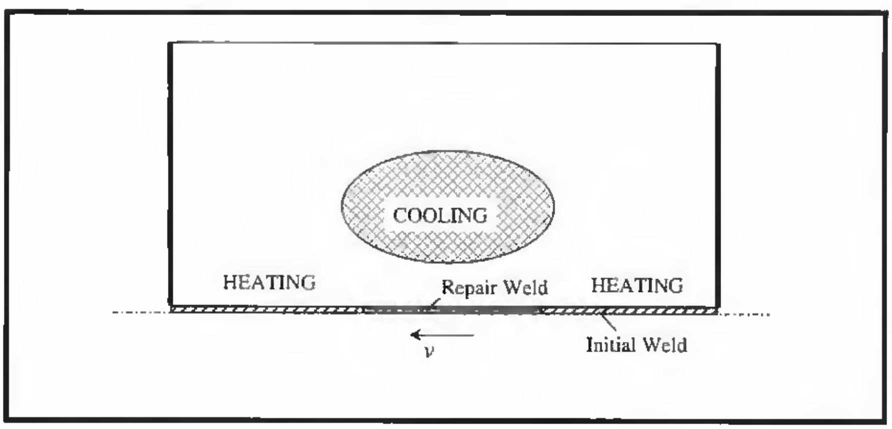

Fig. 10 — Thermal stretching technique for repair welding.

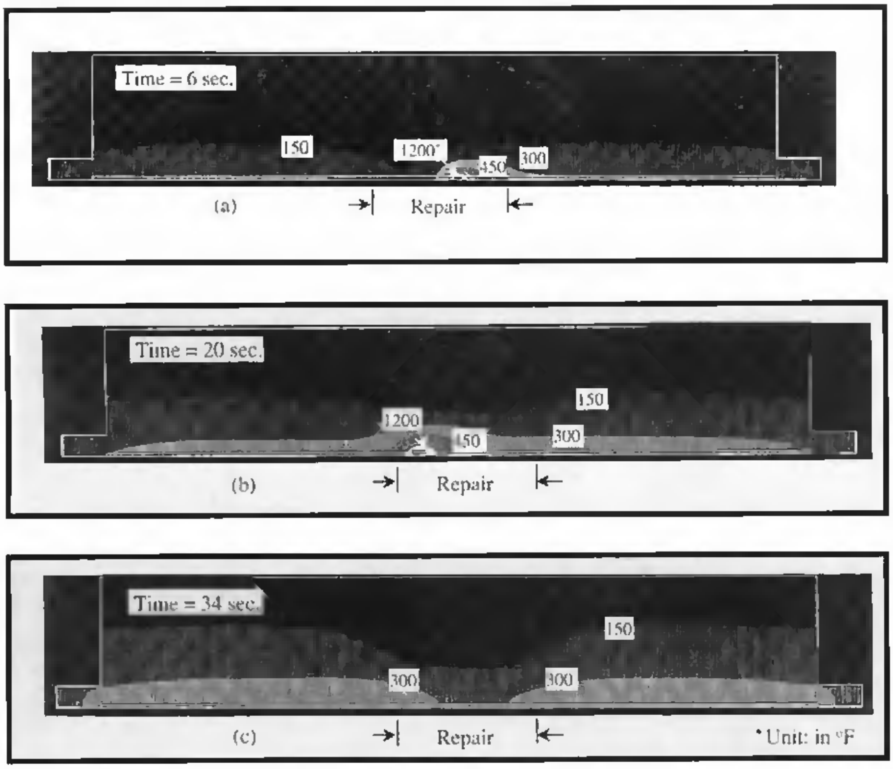

Fig. 11 — Temperature distributions for repair welding with thermal stretching technique. A — 6 s; B — 20 s; C — 34 s.

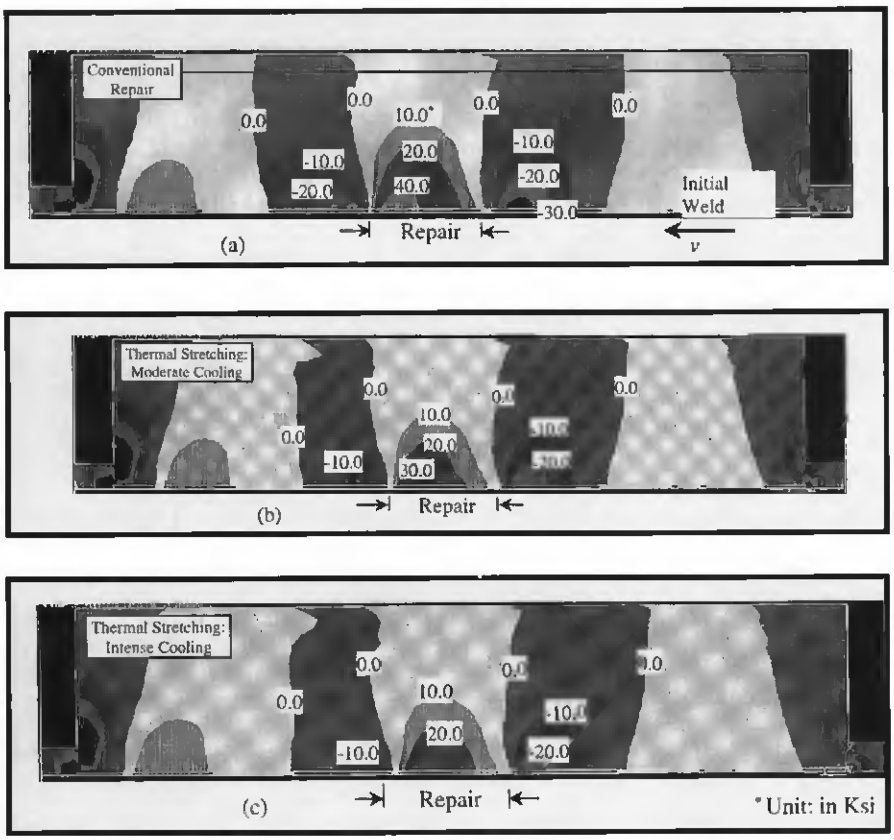

Fig. 12 — Comparison of residual stress distributions. A — Conventional repair; B — thermal stretching with moderate coooling; C — thermal stretching with intense cooling.

utility industry.

In the following, a residual stress mitigation technique is presented based on the detailed knowledge of the weld residual stress development in the repair welds of concern. With a proper combination of stationary heating and cooling as shown in Fig. 10, the heat flow mechanisms during and after repair can be altered to an extent that the plastic compression on heating becomes significantly reduced. As a result, the residual stresses can then be minimized, particularly for the transverse component. The underlying principle is to achieve transverse "stretching" effects on the repair weld by means of the prescribed temperature field. It seems, therefore, appropriate to term such a technique as a "thermal stretching" technique.

Again, the shell element repair model (Fig. 2) was used to demonstrate the effectiveness of this proposed technique. Figure 11 shows the simulated temperature distributions resulting from repair welding with the thermal stretching technique. During repair welding, some slight heating on the initial weld to both the left and right hand sides of the repair weld were noticeable — Figs. 11A and 11B. As soon as the welding arc was terminated, the intense cooling on the region above the repair weld generated a strong depression on the isotherms toward the repair weld (Fig. 11C), exerting stretching effects on the repair weld. The resulting predicted transverse residual stress distributions are given in Fig. 12, where the results for conventional repair welding is shown on the top. Figures 12B and 12C show the results of repair welding with the thermal stretching technique with moderate and intense cooling conditions, respectively. The predicted reduction of the repair weld residual stresses is significant, about 40–50% for an intense cooling source — Fig. 12C. It should be noted that the present arrangement for localized heating and cooling was intended to maximize the stretching effects in the transverse direction so that the transverse residual stresses can be minimized, since the transverse residual stress component was identified as the critical component in subsequent structural integrity assessments (Ref. 22). As a result, the reduction in the longitudinal residual stresses after applying the thermal stretching technique was insignificant.

Conclusions

In this investigation, an advanced finite element procedure involving the use of both a shell/plate element and a 2-D cross-sectional model was used to study 3-D weld residual stress characteristics.

The shell/plate element model was used to capture some of the global residual stress features in both initial welds and repair welds. In the meantime, a 2-D cross-sectional model, with generalized plane-strain conditions that were consistent with the deformation mode at a specified cross section, was used to resolve the local residual stress details. The following observations can be made:

1) Transverse residual stresses in initial welds, although of a relatively low magnitude, exhibit a significant variation along the weld direction. Such variations must be taken into account in order to correctly interpret numerical results from a 2-D model.

2) Highly tensile longitudinal residual stresses are present in a region spanning a few weld widths. Under the present undermatched yield strength conditions, the maximum longitudinal stresses can reach beyond their respective yield strengths.

3) Both longitudinal and transverse residual stresses are highly tensile near and within the repair weld due to severe restraint conditions during repair.

4) To reduce the transverse residual stresses, proper welding procedures can be developed. For present applications, it appears that the thermal stretching technique proposed offers a potentially simple and effective way to reduce the transverse residual stresses for a weld repair.

References

1. Masubuchi, K. 1980. Analysis of welded structures. *International Series on Science and Technology*, 33, New York, N.Y.,Pergamon Press.

2. Ueda, Y., Kim, Y. C., Garatani, K., Yamakita, T., and Bang, H. S. 1986. Mechanical characteristics of repair welds in thick plate: report I — distributions of three-dimensional welding residual stresses and plastic strains and their production mechanisms. *Trans. Japan Weld. Res. Inst.* 15(2):359–368.

3. Kim, Y. D., Yamakita, T., Bang, H. S., and Ueda, Y. 1988. Mechanical characteristics of repair welds in thick plate: report II — validity of two-dimensional plane deformation analysis. *Trans. Japan Weld. Res. Inst.* 17(2): 359–368.

4. Rybicki, E. F., Schmueser, D. W., Stonesifer, R. W., Groom, J. J., and Mishler, H. W. 1978. A finite-element model for residual stress and deflections in girth-butt welded pipes. *ASME Journal of Pressure Vessel Technology* 100: 226–232.

5. Brust, F. W., and Rybicki, E. F. 1981. A computational model of backlay welding for controlling residual stresses in welded pipes. *ASME Journal of Pressure Vessel Technology* 103:226–232.

6. Brust, F. W., and Kanninen, M. F. 1981. Controlling residual stresses by heat sink welding. Battelle Research Reports to Electric Power Research Institute (EPRI), EPRI Report No. NP-2159-LD.

7. Pavelic, V., Tankakuchi, R., Uyehara, O. A., and Myers, P. S. 1969. Experimental and computed temperature histories in gas tungsten arc welding thin plates. *Welding Journal* 48(7): 295-s to 305-s.

8. Anderson, B. A. B. 1978. Thermal stresses in a submerged arc welded joint considering phase transformation. *ASME Journal of Engineering Materials and Technology* 100: 356–362.

9. Friedman, E., and Glickstein, S. S. 1976. An investigation of the thermal response of stationary gas tungsten arc welds. *Welding Journal* 55(12): 408-s to 420-s.

10. Goldak, J., McDill, M., Oddy, A., Bibby, M. J., House, R., and Chi, X. 1986. Computational heat transfer for weld mechanics. *Advances in Welding Science and Technology*, ed. S. A. David, ASM International, Materials Park, Ohio, pp. 15–20.

11. Karlsson, R. I., and Josefson, B. L. 1990. Three-dimensional finite element analysis of temperature and stresses in a single-pass butt-welded pipe. *ASME Journal of Pressure Vessel Technology* 112: 76-84.

12. Choi, J., and Mazumder, J. 1995. Numerical and experimental analysis for solidification and residual stress in the GMAW process for AISI 304 stainless steel. *Proceedings of the 4th International Conference on Trends in Welding Research*, ed. H. B. Smartt, J. A. Johnson and S. A. David, ASM International, Materials Park, Ohio, pp. 75–86.

13. Oddy, A. S., Goldak J. A., and McDill, J. M. J. 1992. Transformation plasticity and residual stresses in single-pass repair welds. *ASME Journal of Pressure Vessel Technology* 114(1): 33–38.

14. Mahin, K. W., Winters, W., Holden, T. M., Hosbons, R. R, and MacEwen, S. R. 1991. Prediction and measurement of residual elastic strain distributions in gas tungsten arc welds. *Welding Journal* 70(9): 245-s to 260-s.

15. Leung, C. K., and Pick, R. J. 1992. Finite element analysis of a multipass weld. *Welding Research Council Bulletin* 356:11–33.

16. Hong, J. K., Dong, P., and Tsai, C. L. 1994. Finite element simulation of residual stresses in multi-pass welds. *International Conference Proceedings on Modeling and Control of Joining Processes*, ed. T. Zacharia, pp. 470–476.

17. Dong, P., *et al.* 1996. Effect of weld residual stresses on crack-opening area analysis of pipes for LBB applications. *ASME Pressure Vessel and Piping Conference Proceedings*, Vol. 2, PVP-Vol. 324, pp. 47–64.

18. Dong, Y., Hong, J. K., Tsai, C. L., and Dong, P. 1997. Finite element modeling of residual stresses in austenitic stainless steel pipe girth welds. *Welding Journal* 76(10): 442-s to 449-s.

19. *ABAQUS*. 1994. User's Manual, Version 5.3, Hibbitt, Karlson & Sorensen, Inc.

20. Brust, F. W., Dong, P. and Zhang, J. 1997. A constitutive model for welding process simulation using finite element methods. *Advances, Computational Engineering Science*, ed. S. N. Atluri and G. Yagawa, pp. 51–56.

21. Zhang, J., Dong, P., and Brust, F. W. 1997. A 3-D composite shell element model for residual stress analysis of multi-pass welds. *Transactions of the 14th International Conference on Structural Mechanics in Reactor Technology* (SMIRT 14), Lyon, France, pp. 335–344.

22. Dong, P., Hong, J. K., Zhang, J., Rogers, P., Bynum, J., and Shah, S. 1998. Effects of repair weld residual stresses on wide-panel specimens loaded in tension. *ASME Journal of Pressure Vessel Technology* 120(2): 122–128.

23. Rogers, P., Bynum, J., and Shah, S. 1998. Wide panel testing technology for evaluating repair weld strengths. *Proceedings of ASME Pressure Vessels and Piping Conference*, San Diego, Calif.

24. Guan, Q., Guo, D. L., and Li, C. Q. 1990. Low Stress Non-Distortion Welding for Aerospace Structures, IIW DOC-1200-90.

25. Michaleris, P., and Sun, X. 1997. Finite element analysis of thermal tensioning techniques mitigation weld buckling distortion. *Welding Journal* 76(11): 451-s to 457-s.